Angular distribution of photoelectrons generated in atomic ionization by twisted radiation

Maksim D. Kiselev *
Skobeltsyn Institute of Nuclear Physics, Lomonosov Moscow State University, 119991 Moscow, Russia;
Faculty of Physics, Lomonosov Moscow State University, 119991 Moscow, Russia;
School of Physics and Engineering, ITMO University, 197101 Saint Petersburg, Russia;
and Laboratory for Modeling of Quantum Processes, Pacific National University, 680035 Khabarovsk, Russia

Elena V. Gryzlova
Skobeltsyn Institute of Nuclear Physics, Lomonosov Moscow State University, 119991 Moscow, Russia

Alexei N. Grum-Grzhimailo
Skobeltsyn Institute of Nuclear Physics, Lomonosov Moscow State University, 119991 Moscow, Russia
and School of Physics and Engineering, ITMO University, 197101 Saint Petersburg, Russia

(Received 13 May 2023; accepted 28 July 2023; published 17 August 2023)

Until recently, theoretical and experimental studies of photoelectron angular distributions (PADs) including nondipole effects in atomic photoionization have been performed mainly for the conventional plane-wave radiation. One can expect, however, that the nondipole contributions to the angular- and polarization-resolved photoionization properties are enhanced if an atomic target is exposed to twisted light. The purpose of the present study is to develop a theory for PADs for the case of twisted light, especially for many-electron atoms. The theoretical analysis is performed for the experimentally relevant case of macroscopic atomic targets, i.e., when the cross-sectional area of the target is larger than the characteristic transversal size of the twisted beam. For such a scenario, we derive expressions for the angular distribution of the emitted photoelectrons under the influence of twisted Bessel beams. As an illustrative example, we consider helium photoionization in the region of the lowest dipole $2s2p\,[^1P_1]$ and quadrupole $2p^2\,[^1D_2]$ autoionization resonances. A noticeable variation of the PAD caused by changing the parameters of the twisted light is predicted.

DOI: 10.1103/PhysRevA.108.023117

I. INTRODUCTION

Studies of photoelectron angular distributions (PADs) are important for many applications and are a fruitful source of fundamental information about the structure of the target and its interaction with the radiation field. Until recently, theoretical analysis of the PADs was based, in accordance with most conventional experimental conditions, on the plane-wave approximation for the vector potential of the radiation field. These studies were promoted to a new level when a twisted light became available in the vacuum ultraviolet (VUV) region [1]. In twisted radiation beams intensity, the profile has a nonuniform structure since the surface of the constant phase differs from a plane and there are complex internal flow patterns [2,3]. Recent developments in technology have made the generation of twisted radiation beams a routine procedure. They can be generated in different ways: with the use of spiral phase plates [4,5], computer-generated holograms [6], q plates [7], axicons [8], integrated ring resonators [9], or on-chip devices [10]. Twisted radiation beams can be generated in a broad range of energies from the optical region to the XUV range [1,11–19]. The following types of twisted beams are mainly considered: Laguerre-Gaussian [20,21] and Bessel [22,23] beams. In the present work, we consider Bessel beams. Experimental (see the review [24]) and theoretical studies are being carried out on the interaction of twisted beams with matter: atoms [25–27], molecules [28,29], and ions [30,31]. The twisting of radiation brings new features into the interaction of the radiation with matter, which at present remain mostly unrevealed but are of great interest. For example, the manifestation of nondipole effects in photoionization may strongly differ from those in the plane-wave case. Thus, a general theory for calculating PADs, especially for many-electron atoms, is required. In [30], a general formalism of ionic photoionization by twisted Bessel light was developed with the use of hydrogenlike wave functions to describe the target system. It allowed one to proceed very far without expanding the field in multipoles. In both cases, i.e., plane-wave and twisted beams, similar sets of field multipoles contribute to the PAD and, despite the fact that the selection rules are modified [32], no radiation multipoles appear in comparison with plane waves. It is important to analyze the dependence of the observable quantities on the geometrical characteristics of the twisted beam and a target. It is known that in the angular distributions of photoelectrons in atomic photoionization, the contribution of a certain interaction multipoles is associated with certain spherical harmonics [33,34]. In photoionization by twisted beams, the PAD changes due to the redistribution of contributions from different multipoles. Thus, it is reasonable to assume that the PAD with twisted radiation exhibits the

*md.kiselev@physics.msu.ru

same structure as in the plane-wave approximation. However, it differs (as will be shown below in present work) by some factors at the spherical harmonics, with these factors depending on the twisted light parameters. If this is the case, the PAD can serve as a diagnostic tool for twisted radiation beams. The photoexcitation of atoms by Bessel beams was already discussed in [35]. The present work is, in this sense, its extension to the case of photoionization.

This article is organized as follows. In Sec. II, we review the general procedure for calculating the PAD in the case of photoionization by plane-wave radiation. Section III is devoted to the development of the mathematical apparatus for calculating the PAD for photoionization by twisted Bessel beams of different polarizations. In Sec. IV, we present an application of the developed approach to the photoionization of helium in the vicinity of the lowest autoionizing resonances, together with a discussion of the PAD transformation near the spectroscopic features of the photoionization cross section when changing the Bessel beam parameters. Unless stated otherwise, we use atomic units throughout.

II. PLANE-WAVE FORMALISM

Consider the atomic photoionization process

$$\hbar\omega + A(\alpha_i J_i M_i) \to A^+(\alpha_f J_f M_f) + e^-(\boldsymbol{p} m_s),$$

where A (A^+) denotes the target atom before (after) ionization by a photon with energy $\hbar\omega$.

Below we show that *any* theoretical analysis of the photoionization of a many-electron atom by twisted light can be carried out using the matrix element

$$M^{(\mathrm{pl})}_{M_i \lambda M_f}(\boldsymbol{k}, \boldsymbol{p}) = \langle \alpha_f J_f M_f,\ \boldsymbol{p} m_s | \hat{R}(\boldsymbol{k}, \lambda) | \alpha_i J_i M_i \rangle, \qquad (1)$$

which describes the photoionization of an atom by a plane-wave photon with wave vector $\boldsymbol{k}$ and helicity $\lambda = \pm 1$. In the matrix element (1), $J_{i,f}$ and $M_{i,f}$ are the total angular momenta and their projections of the initial (before ionization) and final (after ionization) atomic (ionic) states, and $\alpha_{i,f}$ are all other quantum numbers needed for the state specification. The emitted electron is characterized by its momentum $\boldsymbol{p}$ and spin projections m_s onto its propagation direction.

We first recall the well-known formalism for the description of the PAD in the plane-wave photoionization.

Plane-wave matrix element

1. Electron-photon interaction operator

$\hat{R}(\boldsymbol{k}, \lambda)$ in the matrix element (1) is the interaction operator. In many-electron calculations, it can be written as a sum of single-particle operators,

$$\hat{R}(\boldsymbol{k}, \lambda) = \sum_q \boldsymbol{\alpha}_q \boldsymbol{u}_\lambda\, e^{i\boldsymbol{k}\boldsymbol{r}_q}. \qquad (2)$$

Here, $\boldsymbol{r}_q$ specifies the position of the q^{th} electron, $\boldsymbol{u}_\lambda$ is the polarization vector, $\boldsymbol{\alpha}_q$ is the vector of the Dirac matrices for the q^{th} particle, and the summation is taken over all atomic electrons. Note that the operator (2) is written in the relativistic framework for the Coulomb gauge for the electron-photon interaction.

In order to evaluate the matrix element (1) with the operator (2), it is practical to expand $\hat{R}(\boldsymbol{k}, \lambda)$ into electric and magnetic multipole terms that are constructed as irreducible tensors of rank L. For the single-particle operator, this expansion is written as [36]

$$\boldsymbol{\alpha}\boldsymbol{u}_\lambda\, e^{i\boldsymbol{k}\boldsymbol{r}} = \sqrt{2\pi} \sum_{LM} \sum_{p=0,1} i^L \sqrt{2L+1}\, (i\lambda)^p \times D^L_{M\lambda}(\hat{\boldsymbol{k}})\, \boldsymbol{\alpha}\, \boldsymbol{a}^{(p)}_{LM}(\boldsymbol{r}), \qquad (3)$$

where $\hat{\boldsymbol{k}} = (\phi_k, \theta_k, 0)$ defines the direction of the incident (plane-wave) photon, $D^j_{mm'}(\hat{\boldsymbol{k}})$ is the Wigner D-function (see, for example, [37]), and the magnetic ($p = 0$) and electric ($p = 1$) multipole terms are given by

$$\begin{aligned} \boldsymbol{a}^{(p=0)}_{LM}(\boldsymbol{r}) &\equiv \boldsymbol{a}^{(m)}_{LM}(\boldsymbol{r}) = j_L(kr)\, \boldsymbol{T}^M_{L,L}, \\ \boldsymbol{a}^{(p=1)}_{LM}(\boldsymbol{r}) &\equiv \boldsymbol{a}^{(e)}_{LM}(\boldsymbol{r}) = j_{L-1}(kr) \sqrt{\frac{L+1}{2L+1}}\, \boldsymbol{T}^M_{L,L-1} \\ &\quad - j_{L+1}(kr) \sqrt{\frac{L}{2L+1}}\, \boldsymbol{T}^M_{L,L+1}. \end{aligned} \qquad (4)$$

Here, $j_L(x)$ is the spherical Bessel function, $k = |\boldsymbol{k}|$, and the vector spherical harmonics $\boldsymbol{T}^M_{L,\Lambda}$ are irreducible tensors of rank L, resulting from the coupling of the spherical unit vectors $\boldsymbol{e}_m$ ($m = 0, \pm 1$) with the spherical harmonics,

$$\begin{aligned} \boldsymbol{T}^M_{L,\Lambda} &= [Y_\Lambda \otimes \boldsymbol{e}]_{LM} \\ &\equiv \sum_m (\Lambda M - m, 1m \,|\, LM) Y_{\Lambda\, M-m}(\theta, \phi)\, \boldsymbol{e}_m, \end{aligned} \qquad (5)$$

where we used standard notation for the Clebsch-Gordan coefficient and $Y_{lm}(\theta, \phi)$ is the spherical harmonic.

2. Continuum electron state

Besides the electron-photon interaction operator, one needs to expand the wave function of the emitted photoelectron into partial waves [36,38,39],

$$|\boldsymbol{p} m_s\rangle = \sum_{\kappa\mu} i^l\, e^{-i\Delta_\kappa}\, [l] \left(l0, \frac{1}{2} m_s \,\middle|\, j m_s \right) D^j_{\mu m_s}(\hat{\boldsymbol{p}})\, |\epsilon\kappa\mu\rangle, \qquad (6)$$

where the summation runs over the Dirac angular-momentum quantum number $\kappa = \pm(j + 1/2)$ for $l = j \pm 1/2$, with l representing the orbital angular momentum of the electron waves $|\epsilon\kappa\mu\rangle$. In Eq. (6), Δ_κ is the scattering phase, and the spin projection m_s is defined with respect to the propagation direction of photoelectron $\hat{\boldsymbol{p}} = (\phi_p, \theta_p, 0)$. We also introduced the notation $[abc\ldots] \equiv \sqrt{(2a+1)(2b+1)(2c+1)\cdots}$.

To obtain the partial-wave expansion of the *many-electron* scattering states, we use Eq. (6) and apply the standard procedure for coupling two angular momenta,

$$\begin{aligned} &|\alpha_f J_f M_f,\ \boldsymbol{p} m_s\rangle \\ &= \sum_{\kappa\mu} i^l\, e^{-i\Delta_\kappa}\, [l] \left(l0, \frac{1}{2} m_s \,\middle|\, j m_s \right) D^j_{\mu m_s}(\hat{\boldsymbol{p}})\, |\epsilon\kappa\mu\rangle |\alpha_f J_f M_f\rangle \\ &= \sum_{\kappa\mu J_t M_t} i^l\, e^{-i\Delta_\kappa}\, [l] \left(l0, \frac{1}{2} m_s \,|\, j m_s \right) \\ &\quad \times (J_f M_f,\, j\mu \,|\, J_t M_t)\, D^j_{\mu m_s}(\hat{\boldsymbol{p}})\, |(\alpha_f J_f, \epsilon\kappa) J_t M_t\rangle. \end{aligned} \qquad (7)$$

In expression (7), the proper antisymmetrization of the outgoing electron with respect to all bound-state orbitals should be ensured.

3. Evaluation of the plane-wave matrix element

By using Eqs. (2) and (7) and applying the Wigner-Eckart theorem, we obtain the matrix element for the plane-wave photons as

$$M^{(\mathrm{pl})}_{M_i\lambda M_f}(\boldsymbol{k},\boldsymbol{p}) = \sqrt{2\pi}\sum_{LMp}\sum_{\kappa\mu J_t M_t} i^{-l+L}\, e^{i\Delta_\kappa}\,(i\lambda)^p \frac{[l][L]}{[J_t]}\left(l0,\frac{1}{2}m_s\middle|jm_s\right)(J_fM_f,\,j\mu\,|\,J_tM_t)$$
$$\times\,(J_iM_i,LM\,|\,J_tM_t)\,D^{j*}_{\mu m_s}(\hat{\boldsymbol{p}})\,D^{L}_{M\lambda}(\hat{\boldsymbol{k}})\langle(\alpha_fJ_f,\epsilon\kappa)J_t||\sum_q \boldsymbol{\alpha}_q\,\boldsymbol{a}^{(p)}_L(\boldsymbol{r}_q)||\alpha_iJ_i\rangle. \tag{8}$$

For the sake of brevity, we denote the many-body reduced matrix element as

$$\langle(\alpha_fJ_f,\epsilon\kappa)J_t||H_\gamma(pL)||\alpha_iJ_i\rangle = i^{-l}\,e^{i\Delta_\kappa}\,\langle(\alpha_fJ_f,\epsilon\kappa)J_t||\sum_q \boldsymbol{\alpha}_q\,\boldsymbol{a}^{(p)}_L(\boldsymbol{r}_q)||\alpha_iJ_i\rangle. \tag{9}$$

Using (9), we obtain

$$M^{(\mathrm{pl})}_{M_i\lambda M_f}(\boldsymbol{k},\boldsymbol{p}) = \sqrt{2\pi}\sum_{LMp}\sum_{\kappa\mu J_t M_t} i^{L}\,(i\lambda)^p \frac{[lL]}{[J_t]}\left(l0,\frac{1}{2}m_s\middle|jm_s\right)(J_fM_f,\,j\mu\,|\,J_tM_t)$$
$$\times\,(J_iM_i,LM\,|\,J_tM_t)\,D^{j*}_{\mu m_s}(\hat{\boldsymbol{p}})\,D^{L}_{M\lambda}(\hat{\boldsymbol{k}})\langle(\alpha_fJ_f,\epsilon\kappa)J_t||H_\gamma(pL)||\alpha_iJ_i\rangle. \tag{10}$$

4. Photoelectron angular distribution

We assume that the atom is initially unpolarized, and the polarization of the residual ion and the photoelectron spin are not detected. Therefore, we average the PAD over the initial magnetic quantum numbers M_i and sum over the final magnetic quantum numbers M_f and m_s:

$$W^{(\mathrm{pl})}(\theta_p,\phi_p) = \frac{1}{2J_i+1}\sum_{M_iM_fm_s}\left|M^{(\mathrm{pl})}_{M_i\lambda M_f}(\boldsymbol{k},\boldsymbol{p})\right|^2. \tag{11}$$

Defining the z axis as the propagation direction of the incident photons, $D^L_{M\lambda}(\hat{\boldsymbol{k}}) = D^L_{M\lambda}(0,0,0) = \delta_{M\lambda}$. Substituting this into Eqs. (10) and (11), we obtain

$$W(\theta_p,\phi_p) = \frac{2\pi}{2J_i+1}\sum_{\substack{M_iM_fm_s\\ \lambda\lambda'}}\sum_{\substack{Lp\\ L'p'}}\sum_{\substack{\kappa\mu\\ \kappa'\mu'}}\sum_{\substack{J_tM_t\\ J'_tM'_t}} i^{L-L'}[LL'll'][J_tJ'_t]^{-1}(i\lambda)^p(-i\lambda')^{p'}\left(l0,\frac{1}{2}m_s\middle|jm_s\right)\left(l'0,\frac{1}{2}m_s\middle|j'm_s\right)$$
$$\times\,(J_iM_i,L\lambda\,|\,J_tM_t)\,(J_iM_i,L'\lambda'\,|\,J'_tM'_t)(J_fM_f,\,j\mu\,|\,J_tM_t)\,(J_fM_f,\,j'\mu'\,|\,J'_tM'_t)\,D^{j*}_{\mu m_s}(\phi_p,\theta_p,0)\,D^{j'}_{\mu' m_s}(\phi_p,\theta_p,0)$$
$$\times\,\langle(\alpha_fJ_f,\epsilon\kappa)J_t||H_\gamma(pL)||\alpha_iJ_i\rangle\,\langle(\alpha_fJ_f,\epsilon\kappa')J'_t||H_\gamma(p'L')||\alpha_iJ_i\rangle^*. \tag{12}$$

We can further proceed as follows: evaluate the product of two Wigner D-functions; sum over $M_iM_fM_tM'_t$ by using the first equality given in (A.91) of [37]; sum over $\mu\mu'$ using the unitarity of the Clebsch-Gordan coefficients; and sum over m_s using Eq. (A.90) of [37]. After these steps, we finally obtain

$$W(\theta_p,\phi_p) = \frac{2\pi}{2J_i+1}\sum_{kq} D^k_{q0}(\phi_p,\theta_p,0)\sum_{\substack{LpL'p'\\ J_tJ'_t\kappa\kappa'}} i^{L-L'}[LL'll'jj'J_tJ'_t](i\lambda)^p(-i\lambda)^{p'}(-1)^{\lambda+J_i-J_f+\frac{1}{2}}\,(L\lambda,L'-\lambda\,|\,kq)(l0,l'0\,|\,k0)$$
$$\times\begin{Bmatrix} j & j' & k\\ l' & l & \frac{1}{2}\end{Bmatrix}\begin{Bmatrix} J_t & J'_t & k\\ L' & L & J_i\end{Bmatrix}\begin{Bmatrix} J_t & J'_t & k\\ j' & j & J_f\end{Bmatrix}\langle(\alpha_fJ_f,\epsilon\kappa)J_t||H_\gamma(pL)||\alpha_iJ_i\rangle\,\langle(\alpha_fJ_f,\epsilon\kappa')J'_t||H_\gamma(p'L')||\alpha_iJ_i\rangle^*, \tag{13}$$

where constructions in curly brackets are Wigner $6j$-symbols.

The term with $k=0$ in (13) gives us

$$W_0 = \frac{2\pi}{2J_i+1}\sum_{LpJ_t\kappa}|\langle(\alpha_fJ_f,\epsilon\kappa)J_t||H_\gamma(pL)||\alpha_iJ_i\rangle|^2,$$

which, in turn, allows one to calculate the total photoionization cross section as

$$\sigma_0 = \frac{8\pi^2}{2J_i+1}\sum_{LpJ_t\kappa}|\langle(\alpha_fJ_f,\epsilon\kappa)J_t||H_\gamma(pL)||\alpha_iJ_i\rangle|^2. \tag{14}$$

III. TWISTED-WAVE FORMALISM

This section is devoted to the discussion of photoionization by twisted light.

A. Evaluation of the twisted-wave matrix element

We assume that the light is prepared in a so-called Bessel state. In our analysis, the Bessel photon beam propagates along the (quantization) z axis. For this case, the Bessel state

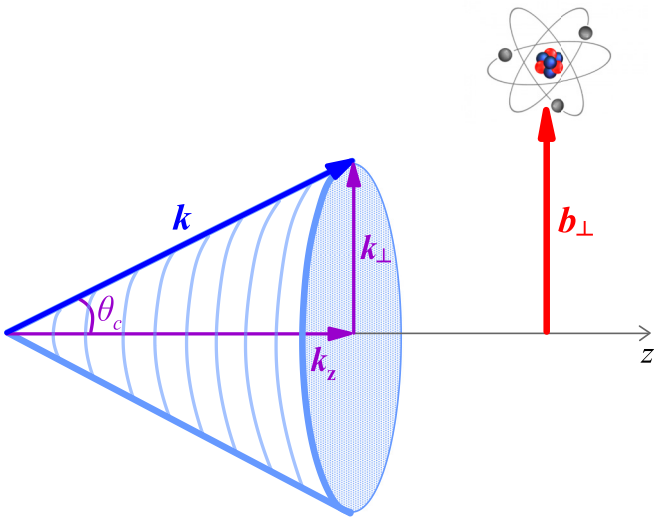

FIG. 1. The overview of the Bessel beam parameters and position of a target atom.

is characterized by the well-defined projections of the linear momentum k_z and the total angular momentum (TAM) onto the z axis, $m_{\rm tam}$. The absolute value of the transverse momentum, $\kappa_\perp = |\mathbf{k}_\perp|$, is fixed; together with k_z, it defines the energy of the photons $\omega = c\sqrt{\kappa_\perp^2 + k_z^2}$. As shown in [30], this Bessel state is described by the vector potential

$$\mathbf{A}^{tw}_{\kappa_\perp m_{\rm tam}\lambda} = \int \mathbf{u}_\lambda e^{i\mathbf{kr}} a_{\kappa_\perp m_{\rm tam}}(\mathbf{k}_\perp)\frac{d^2\mathbf{k}_\perp}{4\pi^2}, \tag{15}$$

where

$$a_{\kappa_\perp m_{\rm tam}}(\mathbf{k}_\perp) = (-i)^{m_{\rm tam}} e^{im_{\rm tam}\phi_k}\sqrt{\frac{2\pi}{k_\perp}}\delta(k_\perp - \kappa_\perp). \tag{16}$$

These expressions present the Bessel state in momentum space as a coherent superposition of plane waves with their wave vectors $\boldsymbol{k} = (\boldsymbol{k}_\perp, k_z)$ lying on the surface of a cone with opening angle $\tan\theta_c = k_\perp/k_z$ (see Fig. 1). Below we characterize the kinematic properties of the Bessel beams by this opening angle.

Using the vector potential (15) and (16), we can derive the matrix element for the photoionization of a many-electron atom by twisted light,

$$M^{(\rm tw)}_{M_i\lambda m_{\rm tam}M_f}(\boldsymbol{p};\theta_c,\,\boldsymbol{b}) = \int a_{\kappa_\perp m_{\rm tam}}(\mathbf{k}_\perp)\, e^{-i\boldsymbol{k}_\perp\boldsymbol{b}_\perp}\, M^{(\rm pl)}_{M_i\lambda M_f}(\boldsymbol{k},\boldsymbol{p})\frac{d^2\mathbf{k}_\perp}{4\pi^2}, \tag{17}$$

where $M^{(\rm pl)}_{M_i\lambda M_f}(\boldsymbol{k},\boldsymbol{p})$ is the conventional plane-wave matrix element (1). We introduced an additional exponential factor $e^{-i\boldsymbol{k}_\perp\boldsymbol{b}_\perp}$ to specify the lateral position of the target atom with regard to the beam axis of the incident light, where the impact parameter $\boldsymbol{b}_\perp = (b_x, b_y)$. This parameter is essential since, in contrast to a plane wave, the Bessel beams have a much more complex internal structure. In particular, their intensity distribution in the transverse direction (the xy plane) is not uniform, but consists of concentric rings of high and low intensity. The direction of the local energy flux also varies significantly within the wavefront. Therefore, one may expect that the properties of the photoelectrons strongly depend on the position $\boldsymbol{b}_\perp$ of the target atom with respect to the Bessel beam axis.

B. Differential cross section for ionization by twisted light

With the help of the "twisted" matrix element (17), one can evaluate the angle-differential photoionization cross section. This cross section depends on both the polarization state of the incident photons and the spatial arrangement of the target. We start our analysis from the simplest case of a *homogeneous macroscopic* target that consists of atoms which are randomly and uniformly distributed within the xy plane. Below we consider the differential cross section for various polarization states of the incident light for such a target.

1. Circularly polarized light

To evaluate the angle-differential cross section for ionization of the macroscopic atomic target by twisted light, we have to average the squared matrix element (17) over the impact parameter,

$$\frac{d\sigma^{(\rm tw,circ)}}{d\Omega_p}(\theta_p,\phi_p;\,\theta_c) = \mathcal{N}\frac{1}{2J_i+1}\sum_{M_iM_fm_s}\int \left|M^{(\rm tw)}_{M_i\lambda m_{\rm tam}M_f}(\boldsymbol{p};\theta_c,\,\boldsymbol{b})\right|^2\frac{d\boldsymbol{b}_\perp}{\pi R^2}. \tag{18}$$

Here, R defines the "size" of the target, which is assumed to be much larger than the characteristic size of the intensity rings in the Bessel beam. We assume that the atom in the initial state is unpolarized and the polarization state of neither the ion nor the electron spin is detected. The evaluation of the prefactor $\mathcal{N}$ is not a trivial task since it requires the redefinition of the concept of a cross section for the case of twisted light. Here we will follow the concept of the cross section defined in Ref. [40].

By inserting the matrix element (17) into Eq. (18) and carrying out the necessary algebra (see Appendix A for details), we obtain the expression for the differential cross section in the case of circularly polarized Bessel light,

$$\begin{aligned}\frac{d\sigma^{(\rm tw,circ)}}{d\Omega_p}(\theta_p,\phi_p;\,\theta_c) = \mathcal{N}\frac{2\pi}{2J_i+1}\sum_J P_J(\cos\theta_p)P_J(\cos\theta_c)\sum_{\kappa\kappa' J_tJ_t'}\sum_{LL'pp'} i^{L-L'}[ll'J_tJ_t'LL'jj'] \\ \times (i\lambda)^{p-p'}(-1)^{\lambda+J_i-J_f+\frac{1}{2}}(L\lambda, L'-\lambda\,|\,J0)\,(l0, l'0\,|\,J0)\begin{Bmatrix} j & j' & J \\ l' & l & \frac{1}{2}\end{Bmatrix}\begin{Bmatrix} J_t & J_t' & J \\ L' & L & J_i\end{Bmatrix}\begin{Bmatrix} J_t & J_t' & J \\ j' & j & J_f\end{Bmatrix} \\ \times \langle(\alpha_fJ_f,\epsilon\kappa)J_t||H_\gamma(pL)||\alpha_iJ_i\rangle\,\langle(\alpha_fJ_f,\epsilon\kappa')J_t'||H_\gamma(p'L')||\alpha_iJ_i\rangle^*,\end{aligned} \tag{19}$$

where $P_n(x)$ is the Legendre polynomial of the $n^{\rm th}$ order.

The limiting case of plane waves may be obtained from (19) by putting $\theta_c = 0$. Then, $P_J(\cos\theta_c) = 1$ and, comparing with (13), we see that these equations coincide. Thus, we obtain a result, which can be formulated as a statement.

Statement 1. For circularly polarized Bessel beams and a homogeneous macroscopic target that consists of atoms which are randomly and uniformly distributed within the plane perpendicular to the beam propagation direction, the effect of twisting on the photoelectron angular distribution is expressed by multiplying each coefficient of the Legendre polynomial $P_k(\cos\theta_p)$ by a factor $P_k(\cos\theta_c)$, where θ_c is the opening angle of the twisted radiation cone. This result is independent of the field multipoles and the target structure.

2. *Linearly polarized light*

In the previous section, we considered the ionization of an atom by a twisted light, characterized by the well-defined values of the TAM projection m_{tam} and the helicity λ. The paraxial limit with additional condition $k_\perp \to 0$ corresponds to the well-known case of *circularly* polarized plane-wave light. Now we turn to the case that can be considered as a twisted *analogon* of plane-wave linearly polarized light. The vector potential of twisted light that is "linearly polarized" in the xz plane can be written as [41]

$$\mathbf{A}^{\rm tw}_{\kappa_\perp\parallel} = \frac{i}{\sqrt{2}}\left(\mathbf{A}^{\rm tw}_{\kappa_\perp m_{\mathsf{tam}}=m+1,\,\lambda=+1} - \mathbf{A}^{\rm tw}_{\kappa_\perp m_{\mathsf{tam}}=m-1,\,\lambda=-1}\right), \quad (20)$$

i.e., as the difference of two vector potentials (15), obtained for different TAM projections and different helicities. The physical meaning of Eq. (20) becomes more transparent if one writes this expression in the paraxial regime,

$$\mathbf{A}^{\rm tw}_{\kappa_\perp\parallel} \approx \boldsymbol{e}_x\, J_m(\kappa_\perp r_\perp)\, e^{im\phi}\, e^{ik_z z}, \quad (21)$$

where we applied the approach from Ref. [30]. Here, m can be considered as the projection of the light's orbital angular momentum (OAM), $m_{\rm oam}$. Applying, additionally, that $k_\perp \to 0$, Eq. (21) transforms to the conventional plane wave linearly polarized in the xz plane: $\mathbf{A}^{\rm tw}_{\kappa_\perp\parallel} \approx \boldsymbol{e}_x\, e^{ik_z z}$.

Here and below, the Bessel light with vector potential (20) is addressed as linearly polarized, and one should take this term in the following sense. The pattern of polarization of such light has a quite complicated structure for large values of θ_c and only for small values of θ_c reduces to the linear polarization in a conventional meaning. Thus, throughout this paper, the term "linearly polarized Bessel (twisted) light" should be understood as "Bessel (twisted) light with the vector potential (20)" and without any restrictions regarding parameter θ_c. Interesting ideas and discussions on the polarization structure complexity can be obtained from [42].

Using the general expression for the vector potential of linearly polarized radiation (20) allows us to derive the photoionization matrix element,

$$M^{\rm (tw)}_{M_i M_f\,\parallel}(\boldsymbol{p};\theta_c,\,\boldsymbol{b}) = \frac{i}{\sqrt{2}}\left(M^{\rm (tw)}_{M_i\lambda=+1\,m_{\mathsf{tam}}=m+1\,M_f}(\boldsymbol{p};\theta_c,\,\boldsymbol{b}) - M^{\rm (tw)}_{M_i\lambda=-1\,m_{\mathsf{tam}}=m-1\,M_f}(\boldsymbol{p};\theta_c,\,\boldsymbol{b})\right), \quad (22)$$

in terms of the matrix elements (17). Applying this expression and performing algebra similar to that in the previous section, we can derive the differential cross section for the ionization by "linearly polarized" twisted light,

$$\frac{d\sigma^{\rm (tw,lin)}}{d\Omega_p}(\theta_p,\phi_p;\,\theta_c) = \mathcal{N}\frac{1}{2J_i+1}\sum_{M_iM_fm_s}\int \left|M^{\rm (tw)}_{M_iM_f\,\parallel}(\boldsymbol{p};\theta_c,\,\boldsymbol{b})\right|^2 \frac{d\boldsymbol{b}_\perp}{\pi R^2}$$
$$= \mathcal{N}\frac{1}{2J_i+1}\sum_{M_iM_fm_s}\sum_{\lambda,\lambda'}\int M^{\rm (pl)}_{M_i\,\lambda\,M_f}(\boldsymbol{k},\boldsymbol{p})\, M^{\rm (pl)*}_{M_i\,\lambda'\,M_f}(\boldsymbol{k},\boldsymbol{p})\, e^{i(\lambda-\lambda')\varphi_k}\,\frac{d\varphi_k}{2\pi}. \quad (23)$$

For $\theta_c \to 0$, this expression reduces to the well-known plane-wave result. Indeed, by using the asymptotic expression for the Wigner D-function,

$$D^L_{M\lambda}(\varphi_k,\theta_c,0) \approx e^{-i\lambda\varphi_k}\,\delta_{\lambda M}, \quad (24)$$

we can write the plane-wave photoionization matrix element as

$$M^{\rm (pl)}_{M_i\,\lambda\,M_f}(\boldsymbol{k},\boldsymbol{p}) \equiv M^{\rm (pl)}_{M_i\,\lambda\,M_f}(\theta_c,\varphi_k,\boldsymbol{p}) \approx e^{-i\lambda\varphi_k} M^{\rm (pl)}_{M_i\,\lambda\,M_f}(\theta_c=0,\varphi_k=0,\boldsymbol{p}) \equiv e^{-i\lambda\varphi_k}\, M^{\rm (pl)}_{M_i\,\lambda\,M_f}(0,\boldsymbol{p}), \quad (25)$$

where the last matrix element describes plane-wave radiation propagating along the quantization z axis. Substituting Eq. (25) into Eq. (23), we obtain

$$\frac{d\sigma^{\rm (pl,lin)}}{d\Omega_p}(\theta_p,\phi_p;\,\theta_c) = \mathcal{N}\frac{1}{2J_i+1}\sum_{M_iM_fm_s}\sum_{\lambda,\lambda'} M^{\rm (pl)}_{M_i\,\lambda\,M_f}(0,\boldsymbol{p}) M^{\rm (pl)*}_{M_i\,\lambda'\,M_f}(0,\boldsymbol{p}). \quad (26)$$

To simplify Eq. (23), we first substitute the matrix elements (10) and, after further transformations (see Appendix B for details), we obtain the expression for the differential cross section in the case of linearly polarized Bessel light,

$$\frac{d\sigma^{\rm (tw,lin)}}{d\Omega_p}(\theta_p,\phi_p;\,\theta_c) = \mathcal{N}\frac{2\pi}{2J_i+1}\sum_J\sum_{M=0,\pm2}\sqrt{\frac{4\pi}{2J+1}}Y^*_{JM}(\theta_p,\phi_p)\, d^J_{MM}(\theta_c)\sum_{\lambda,\lambda'}\delta_{M,\lambda-\lambda'}$$
$$\times\sum_{\kappa\kappa' J_t J_t'}\sum_{LL'pp'} i^{L-L'}(i\lambda)^p(-i\lambda')^{p'}(-1)^{\lambda+J_i-J_f+\frac{1}{2}}[ll'LL'J_tJ_t'jj'](l0,l'0\,|\,J0)(L\lambda,L'-\lambda'\,|\,JM)$$

$$\times \begin{Bmatrix} j & j' & J \\ l' & l & \frac{1}{2} \end{Bmatrix} \begin{Bmatrix} J_t & J_t' & J \\ L' & L & J_i \end{Bmatrix} \begin{Bmatrix} J_t & J_t' & J \\ j' & j & J_f \end{Bmatrix} \langle (\alpha_f J_f, \epsilon\kappa) J_t || H_\gamma(pL) || \alpha_i J_i \rangle \langle (\alpha_f J_f, \epsilon\kappa') J_t' || H_\gamma(p'L') || \alpha_i J_i \rangle^*. \quad (27)$$

In Eq. (27), $d^j_{mm'}(\theta)$ is the small Wigner D-function, [37]. For $\theta_c = 0$, $d^J_{MM}(0) = 1$, and thus we can make a second statement.

Statement 2. For "linearly polarized" Bessel beams and a homogeneous macroscopic target that consists of atoms which are randomly and uniformly distributed within the plane perpendicular to the beam propagation direction, the effect of twisting on the photoelectron angular distribution is expressed by multiplying each coefficient of the spherical harmonic $Y_{kq}(\theta_p, \phi_p)$ by a factor $d^k_{qq}(\theta_c)$, where θ_c is the opening angle of the twisted radiation cone. The result is independent of the field multipoles and the atomic structure.

Equations (13), (19), and (27) are written in the jj-coupling scheme. The transformation to a nonrelativistic LL-coupling scheme is quite simple: one has to replace $J_{i,f,t}$ with $L_{i,f,t}$; replace j with l; replace $1/2$ in the phase with zero; and replace Wigner $6j$-symbol $\left\{ \begin{smallmatrix} j & j' & J \\ l' & l & \frac{1}{2} \end{smallmatrix} \right\}$ with 1.

IV. RESULTS AND DISCUSSION

The main consequence of Statements 1 and 2 is the possibility to use the well-known parametrization of the PADs in photoionization by plane-wave radiation in terms of the anisotropy parameters β, γ, and δ [33] also for the case of photoionization by twisted radiation. The difference between "plane" and "twisted" PADs comes down to geometrical multipliers depending on the angle of the twisted radiation cone θ_c, while the anisotropy parameters remain unaffected. This makes it possible to calculate them by different methods and models. It also means that one may expect a more pronounced change in the PAD when at least one of the anisotropy parameters changes significantly.

For an illustration of our ideas, we now consider photoionization of the helium atom in the vicinity of the lowest autoionization states (AIS): dipole $2s2p\,[^1P_1]$ and quadrupole $2p^2\,[^1D_2]$, respectively. The calculation of the dipole and quadrupole photoionization amplitudes was performed by means of the B-spline R-matrix code [43] within the LS-coupling scheme to describe the initial atomic and final ionic states. All the wave functions were obtained by the multiconfiguration Hartree-Fock method using the MCHF code [44]. For the initial state, we first performed a Hartree-Fock (HF) optimization of the $1s^2\,[^1S]$ state in order to obtain a first approximation of the $1s$ orbital. Then we added the configurations of the same parity, $1s2s, 1s3s, 2s^2, 2s3s, 2p^2, 2p3p, 3p^2, 3d^2$, to the ground-state description, optimizing all of them together on the ^1S term. For the six final ionic states (targets), we used single-configuration representations $1s\,[^2S]$, $2s\,[^2S]$, $2p\,[^2P]$, $3s\,[^2S]$, $3p\,[^2P]$, $3d\,[^2D]$. The dipole and quadrupole photoionization cross sections are presented in Fig. 2(a).

It is well known that for ionization of an s shell, $\beta = 2$ and $\delta = 0$. Therefore, γ remains the only parameter that may change with the photon energy. The nondipole parameter γ characterizes the interference between the electric dipole ($E1$) and quadrupole ($E2$) photoionization amplitudes. One should expect the sharpest modulation of this parameter when the $E2$ photoionization cross section becomes comparable to or even dominates $E1$ photoionization. For example, such a situation is observed in helium photoionization near the dipole $2s2p\,[^1P_1]$ and quadrupole $2p^2\,[^1D_2]$ AIS resonances. At the photon energy of ≈60.18 eV, the cross section of the $E1$ dipole photoionization approaches zero, i.e., $\sim 10^{-4}$ Mb. Hence the $E2$ quadrupole photoionization dominates in this region [see Fig. 2(a)].

The photon energy dependence of γ is presented in Fig. 2(b), together with experimental data points from [45]. Comparison of the present theoretical results with experimental data shows a significant discrepancy around 60.2 eV. This issue was extensively studied in [46]. The most probable and plausible reason for such a difference is an underestimation of the background signal, i.e., an entirely instrumental origin

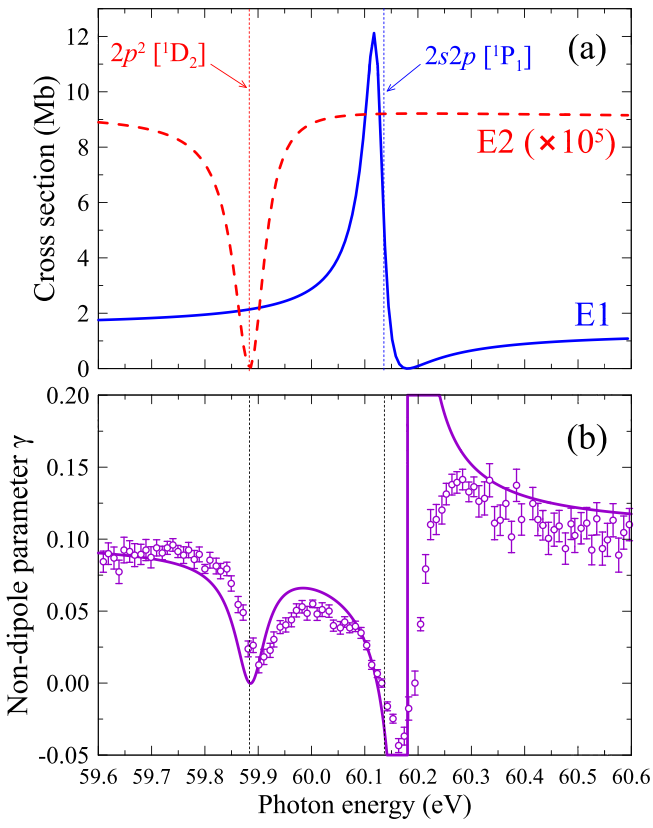

FIG. 2. (a) Cross sections for dipole $E1$ (solid blue line) and quadrupole $E2$ (red dashed line) photoionization of helium obtained using Eq. (14) for a particular multipole. (b) Nondipole parameter γ of the photoelectron angular distribution. The solid line represents the theoretical prediction; the open circles are the experimental data from [45].

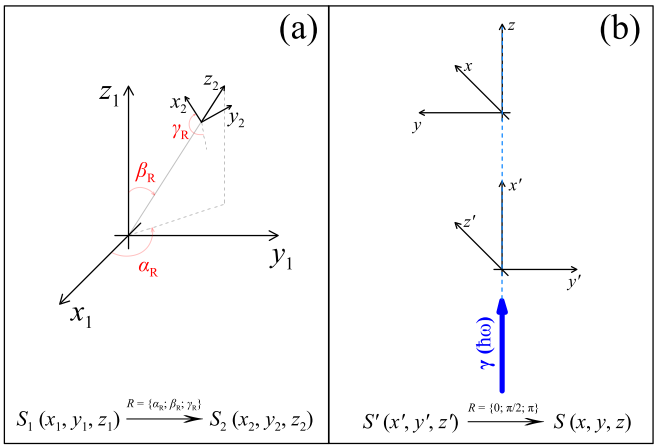

FIG. 3. (a) General transformation between coordinate systems S_1 and S_2 by the Euler angle rotation $R = \{\alpha_R; \beta_R; \gamma_R\}$. (b) The transformation between the coordinate systems S' [used in Eq. (28)] and S [used in Eq. (30)] is provided by $R = \{0; \pi/2; \pi\}$.

during the experimental data processing. The spectroscopic models, however, appear to be reliable.

In order to evaluate the expression for the PAD resulting from twisted wave photoionization, we start from the well-known plane-wave nonrelativistic PAD in the general form within first-order nondipole corrections [47]. We choose the coordinate system S' (see Fig. 3) in such a way that the x' axis is the propagation axis of the light beam ($\boldsymbol{k} \parallel x'$) and the z' axis is the polarization axis,

$$\left(\frac{d\sigma}{d\Omega}\right)_{S'} = \frac{\sigma_0}{4\pi}\left[\left(1 + \frac{\beta}{4} - \frac{3}{4}P\beta + \frac{3}{2}P\beta\cos^2\theta'_p\right) + \left(\delta + \gamma P\cos^2\theta'_p - \gamma\frac{P-1}{2}\right)\sin\theta'_p\cos\phi'_p + \frac{3\beta}{4}(P-1)(\sin\theta'_p\cos\phi'_p)^2 + \gamma\frac{P-1}{2}(\sin\theta'_p\cos\phi'_p)^3\right]. \tag{28}$$

Here, P is the degree of linear polarization. $P = 1$ in Eq. (28) corresponds to the case of linearly polarized light, while $P = 0$ corresponds to the case of circularly polarized light. For convenience, one can express all the combinations of sines and cosines in Eq. (28) in terms of spherical harmonics $Y_{lm}(\theta'_p, \phi'_p)$. To apply the statements obtained in Sec. III, we need to transform Eq. (28) from the coordinate system S' to S, where the x axis is the polarization axis and the z axis is the propagation direction. The conversion of spherical harmonics when the coordinate system undergoes rotation described by the triad of Euler angles $R = \{\alpha_R; \beta_R; \gamma_R\}$ is given by [37]

$$Y_{KQ'}(\theta'_p, \phi'_p) = \sum_Q D^K_{QQ'}(\alpha_R; \beta_R; \gamma_R) Y_{KQ}(\theta_p, \phi_p). \tag{29}$$

The transformation $S' \to S\,(z' \to x;\, x' \to z)$ is provided by the rotation $R = \{0; \frac{\pi}{2}; \pi\}$. The transformation of Eq. (28) then leads to

$$\left(\frac{d\sigma}{d\Omega}\right)_S = \frac{\sigma_0}{4\pi}\left(1 - \frac{\beta}{2}\sqrt{\frac{4\pi}{5}}\left\{Y_{20}(\theta_p, \phi_p) - \frac{P\sqrt{6}}{2}[Y_{2-2}(\theta_p, \phi_p) + Y_{2+2}(\theta_p, \phi_p)]\right\} + \left(\delta + \frac{\gamma}{5}\right)\sqrt{\frac{4\pi}{3}}Y_{10}(\theta_p, \phi_p) - \frac{\gamma}{5}\sqrt{\frac{4\pi}{7}}\left\{Y_{30}(\theta_p, \phi_p) - P\sqrt{\frac{5}{6}}[Y_{3-2}(\theta_p, \phi_p) + Y_{3+2}(\theta_p, \phi_p)]\right\}\right). \tag{30}$$

Equation (30) is the starting point for analyzing PADs generated in helium photoionization by twisted radiation. Figures 4(a)–4(c) present calculated PADs with $P = 0$ and $P = 1$ for three different photon energies: 59.8 eV (below the resonance), 60.178 eV (just below the minimum in the $2s2p[^1P_1]$ dipole resonance), and 60.18 eV (exactly at the minimum).

In our further analysis, we follow the order of considerations in Sec. III and hence begin with circularly polarized twisted radiation. We assume $P = 0$ in Eq. (30) and multiply each spherical harmonic $Y_{kq}(\theta_p, \phi_p)$ by the factor $d^k_{qq}(\theta_c)$ according to Statement 1. Although the statement refers to the Legendre polynomials, for $P = 0$, Eq. (30) contains only spherical harmonics $Y_{kq}(\theta_p, \phi_p)$ with $q = 0$, which are equivalent to the Legendre polynomials. After such a transformation, we obtain the dependence of the PAD on the twisted radiation cone angle θ_c. Simulated PADs for different values of θ_c are presented in Figs. 4(d)–4(f). It is clearly seen that the PADs are very sensitive to both the photon energy and the angle θ_c. For $\omega = 59.8$ eV in plane-wave photoionization, the angular distribution is "purely" dipole. Increasing θ_c leads to gains in the forward-backward direction and the PAD becomes almost isotropic. Closer to the minimum of the dipole resonance ($\omega = 60.178$ eV), the PADs start to lose the general symmetry because of the amplification of nondipole effects. Exactly in the minimum ($\omega = 60.18$ eV according to our calculations), the shape of the PADs becomes qualitatively different. Specifically, a predominant portion of photoelectrons is emitted in the direction of the incident beam wave vector $\boldsymbol{k}$ and a small fraction in the opposite direction.

Next we consider the linearly polarized case, set $P = 1$ in Eq. (30), and multiply each spherical harmonic $Y_{kq}(\theta_p, \phi_p)$ by the factor $d^k_{qq}(\theta_c)$ according to Statement 2. Calculated PADs for this case are presented in Figs. 4(g)–4(i). For $\omega = 59.8$ eV, the evolutions of the PADs with increasing θ_c do not show any striking changes, becoming only more intense in the forward-backward direction. On the contrary, a little below the dipole resonance minimum ($\omega = 60.178$ eV), the angular distribution changes quite noticeably and a redistribution of photoelectrons occurs. Finally, when the photon energy approaches the minimum at $\omega = 60.18$ eV for the case of linearly polarized twisted light, we find significant changes in

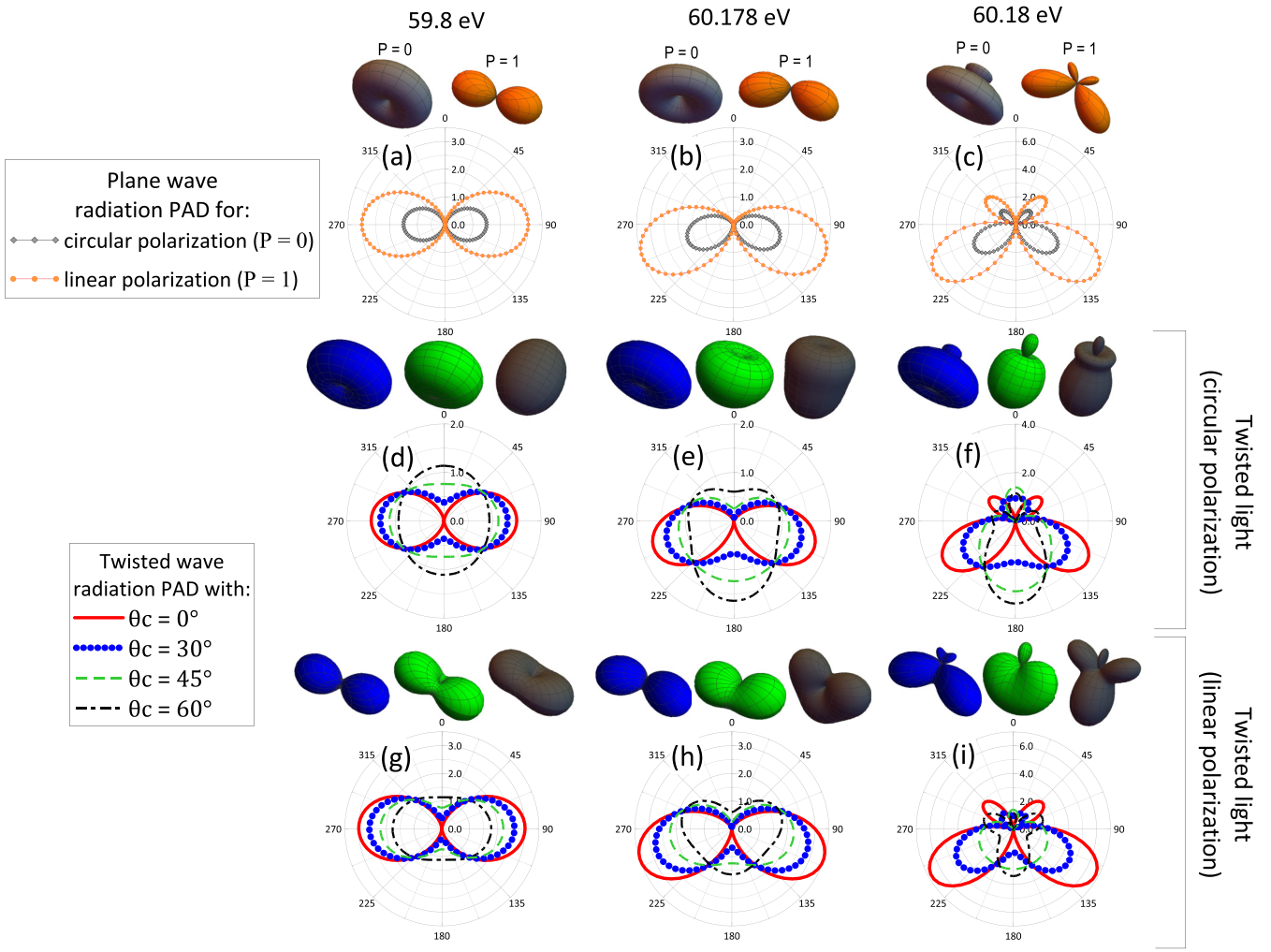

FIG. 4. (a)–(c) Simulated, according to Eq. (30), PADs for plane-wave photoionization of helium (diamonds and circles along the line indicate the angular grid step). The upper part shows three-dimensional (3D) views of the angular distributions for circularly polarized ($P = 0$, gray one on the left) and linearly polarized ($P = 1$, orange one on the right) light. (d)–(f) Simulated, according to Statement 1, PADs for twisted circularly polarized Bessel beam photoionization of helium for different values of θ_c. The upper part shows 3D views of the angular distributions for $\theta_c = 30^\circ$, 45°, and 60° (from left to right). (g)–(i) Simulated, according to Statement 2, PADs for twisted linearly polarized Bessel beam photoionization of helium for different values of θ_c. The upper part shows 3D views of the angular distributions for $\theta_c = 30^\circ$, 45°, and 60° (from left to right). Note that all the polar plots correspond to the case of $\theta_p = 0$. The angular grid step for the PADs in (d)–(i) is similar to that in (a)–(c). The columns correspond to the photon energy indicated at the top of the figure: (a), (d), (g) $\omega = 59.8$ eV; (b), (e), (h) $\omega = 60.178$ eV; (c), (f), (i) $\omega = 60.18$ eV.

the shape of the PADs for different values of θ_c. For $\theta_c = 30^\circ$, for example, there are two dominant petals in the forward direction and two minor ones in the backward direction. Turning to $\theta_c = 45^\circ$ merges the two backward petals into one and redistributes photoelectrons in the forward direction by filling the local minimum along the incident beam wave vector $\boldsymbol{k}$. For $\theta_c = 60^\circ$, two additional dominant backward directions of electron emission are formed ($\sim 67.5^\circ$ and 290.5°), and in the forward direction, the strengthening trend along the wave vector $\boldsymbol{k}$ continues.

Summing up, the above analysis showed that the angular distributions of photoelectrons emitted under the influence of a twisted Bessel beam are very sensitive to the parameters of the incident radiation (polarization and cone angle θ_c) in the energy regions where a strong domination of nondipole effects occurs. Hence, one can control the shape of the PAD by manipulating the polarization and twisted radiation cone opening angle θ_c.

From the above, it is clear that experimental angular distributions of high accuracy could serve as a tool to extract the parameters of twisted beams, i.e., one can diagnose the incident twisted radiation beam. Applying Statement 1 to Eq. (30) for the case of a circularly polarized ($P = 0$) twisted beam and writing it in terms of Legendre polynomials, we obtain, for the PAD,

$$\left(\frac{d\sigma^{(\mathrm{tw,circ})}}{d\Omega}\right)_S = \frac{\sigma_0}{4\pi}\Big[1 - \frac{\beta}{2}P_2(\cos\theta_p)P_2(\cos\theta_c) + \Big(\delta + \frac{\gamma}{5}\Big)P_1(\cos\theta_p)P_1(\cos\theta_c) - \frac{\gamma}{5}P_3(\cos\theta_p)P_3(\cos\theta_c)\Big]. \quad (31)$$

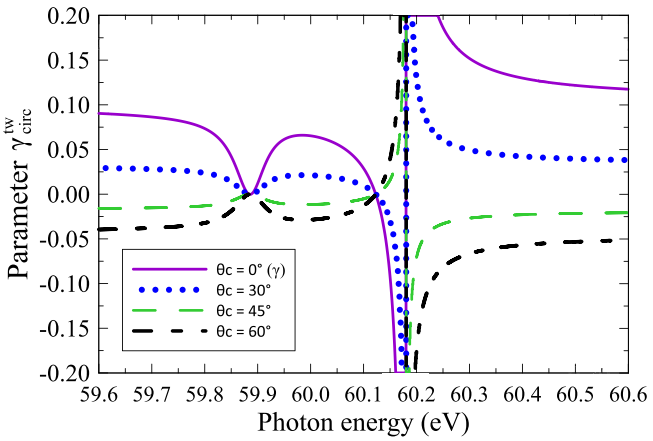

FIG. 5. Calculated parametrization factor $\gamma_{\rm circ}^{\rm tw}$ from Eq. (35) for different values of the twisted beam cone angle θ_c for helium photoionization. For $\theta_c = 0^\circ$, the factor $\gamma_{\rm circ}^{\rm tw}$ coincides with the conventional nondipole parameter γ depicted in Fig. 2(b).

Putting

$$\beta_{\rm circ}^{\rm tw} = \beta P_2(\cos\theta_c), \tag{32}$$

$$\gamma_{\rm circ}^{\rm tw} = \gamma P_3(\cos\theta_c), \tag{33}$$

$$\delta_{\rm circ}^{\rm tw} = \left(\delta + \frac{\gamma}{5}\right)P_1(\cos\theta_c) - \frac{\gamma}{5}P_3(\cos\theta_c), \tag{34}$$

equation (31) can be parameterized as

$$\left(\frac{d\sigma^{\rm (tw,circ)}}{d\Omega}\right)_S = \frac{\sigma_0}{4\pi}\left[1 - \frac{\beta_{\rm circ}^{\rm tw}}{2}P_2(\cos\theta_p) + \left(\delta_{\rm circ}^{\rm tw} + \frac{\gamma_{\rm circ}^{\rm tw}}{5}\right)P_1(\cos\theta_p) - \frac{\gamma_{\rm circ}^{\rm tw}}{5}P_3(\cos\theta_p)\right]. \tag{35}$$

Equation (35) has the same structure as the PAD for photoionization by plane-wave circularly polarized radiation. Therefore, if one performs an experiment on photoionization by both plane and twisted (Bessel) radiation with the same target atom and extracts the anisotropy parameters β, $\beta_{\rm circ}^{\rm tw}$, γ, $\gamma_{\rm circ}^{\rm tw}$, δ, and $\delta_{\rm circ}^{\rm tw}$, then it becomes possible to diagnose the Bessel beam, i.e., either to find [according to parametrizations (32)–(34)] its parameter θ_c, if it is unknown for some reason, or to estimate the quality of the twisted beam preparation by comparing the expected and the experimentally derived values of θ_c. The dependence of $\gamma_{\rm circ}^{\rm tw}$ on the twisted cone angle θ_c is presented in Fig. 5.

V. CONCLUSIONS

In the present work, we performed a theoretical analysis of the photoionization process caused by twisted radiation, specifically, Bessel beams. Assuming the atomic target to be extended (the size of the target area is larger than the characteristic size of the incident beam), we proved two statements that allow one to derive an expression for the PADs under the influence of twisted light of different polarization. Being extensions of the well-known parametrizations for the plane-wave radiation, our "twisted" expressions will help to plan and to perform next-generation atomic photoionization experiments.

An illustration of the statements' application was given for the example of helium atoms ionized by twisted radiation in the vicinity of the lowest autoionization resonances in dipole and quadrupole photoionization. When nondipole effects become dominating, the shape of the PAD noticeably changes. Moreover, increasing the opening angle, i.e., the parameter θ_c for different incident photon energies, substantially modifies the PADs. The latter result suggests that the angular distributions can be controlled by the twisted radiation parameters. In addition, we showed that the PADs can serve as a diagnostic tool for the parameters of the incident circular polarized twisted Bessel radiation because of the possibility to parametrize the angular distribution expressions accordingly.

ACKNOWLEDGMENTS

The authors benefited greatly from discussions with A. Surzhykov and acknowledge K. Bartschat for careful reading of the manuscript and useful suggestions. The work on the development of formalism for the twisted light interaction with many-electron atoms and analysis of photoelectron angular distributions in helium ionization by the Bessel light were funded by the Russian Science Foundation (Project No. 21-42-04412, [48]). The calculations of the photoionization amplitudes were performed using resources of the Shared Services "Data Center of the Far-Eastern Branch of the Russian Academy of Sciences" and supported by the Ministry of Science and Higher Education of the Russian Federation (Project No. 0818-2020-0005).

APPENDIX A: DIFFERENTIAL CROSS SECTION FOR CIRCULARLY POLARIZED BESSEL LIGHT

By inserting the matrix element (17) into Eq. (18), we obtain

$$\frac{d\sigma^{\rm (tw,circ)}}{d\Omega_p}(\theta_p,\phi_p;\theta_c) = \mathcal{N}\frac{1}{2J_i+1}\sum_{M_iM_fm_s}\int e^{i(\boldsymbol{k}'_\perp-\boldsymbol{k}_\perp)\boldsymbol{b}_\perp}\, a_{\kappa_\perp m_{\rm tam}}(\mathbf{k}_\perp)\, a^*_{\kappa_\perp m_{\rm tam}}(\mathbf{k}'_\perp) M^{\rm (pl)}_{M_i\lambda M_f}(\boldsymbol{k},\boldsymbol{p})\, M^{\rm (pl)*}_{M_i\lambda M_f}(\boldsymbol{k}',\boldsymbol{p})\frac{d^2\mathbf{k}_\perp}{4\pi^2}\frac{d^2\mathbf{k}'_\perp}{4\pi^2}\frac{d\boldsymbol{b}_\perp}{\pi R^2}$$

$$= \mathcal{N}\frac{1}{2J_i+1}\sum_{M_iM_fm_s}\int \left|a_{\kappa_\perp m_{\rm tam}}(\mathbf{k}_\perp)\right|^2 \left|M^{\rm (pl)}_{M_i\lambda M_f}(\boldsymbol{k},\boldsymbol{p})\right|^2 \frac{d^2\mathbf{k}_\perp}{4\pi^2}. \tag{A1}$$

By using the explicit form of the amplitude $a_{\kappa_\perp m_{\rm tam}}(\mathbf{k}_\perp)$ and the relation $|\delta(k_\perp-\kappa_\perp)|^2 = R/\pi\,\delta(k_\perp-\kappa_\perp)$ (cf. Eq. (24) from Ref. [40]), we finally obtain

$$\frac{d\sigma^{(\mathrm{tw,circ})}}{d\Omega_p}(\theta_p,\phi_p;\,\theta_c) = \mathcal{N}\frac{1}{2J_i+1}\sum_{M_iM_fm_s}\int \left|M^{(\mathrm{pl})}_{M_i\lambda M_f}(\boldsymbol{k},\boldsymbol{p})\right|^2\frac{d\varphi_k}{2\pi}. \tag{A2}$$

Here, the plane-wave matrix element $M^{(\mathrm{pl})}_{M_i\lambda M_f}(\boldsymbol{k},\boldsymbol{p})$ is calculated for the photon wave vector $\boldsymbol{k} = k(\sin\theta_c\cos\varphi_k,\ \sin\theta_c\sin\varphi_k,\ \cos\theta_c)$, with $k = c\omega$ and θ_c as input parameters.

One can perform the integration over the azimuthal angle φ_k analytically if one rewrites the plane-wave matrix element (10) as

$$M^{(\mathrm{pl})}_{M_i\lambda M_f}(\boldsymbol{k},\boldsymbol{p}) = \sum_{LMp}(i\lambda)^p\,D^L_{M\lambda}(\hat{\boldsymbol{k}})\,G_{LM}(\boldsymbol{p}), \tag{A3}$$

where we introduced

$$G_{LM}(\boldsymbol{p}) = \sqrt{2\pi}\,i^L\sum_{\kappa\mu}\sum_{J_tM_t}\frac{[lL]}{[J_t]}\left(l0,\,\frac{1}{2}m_s\,\middle|\,jm_s\right)D^{j*}_{\mu m_s}(\hat{\boldsymbol{p}})(J_fM_f,\,j\mu\,|\,J_tM_t)\,(J_iM_i,LM\,|\,J_tM_t)\langle(\alpha_fJ_f,\epsilon\kappa)J_t||H_\gamma(pL)||\alpha_iJ_i\rangle. \tag{A4}$$

By inserting (A4) into (A3) and using the relation $\int_0^\infty e^{i(M-M')\varphi_k}d\varphi_k = 2\pi\delta_{MM'}$, we obtain

$$\frac{d\sigma^{(\mathrm{tw,circ})}}{d\Omega_p}(\theta_p,\phi_p;\,\theta_c) = \mathcal{N}\frac{1}{2J_i+1}\sum_{M_iM_fm_s}\sum_{LL'pp'}\sum_{M}(i\lambda)^{p-p'}d^L_{M\lambda}(\theta_c)\,d^{L'}_{M\lambda}(\theta_c)G_{LM}(\boldsymbol{p})\,G^*_{L'M}(\boldsymbol{p}). \tag{A5}$$

To find a more practical expression, we write Eq. (A5) in the form

$$\begin{aligned}\frac{d\sigma^{(\mathrm{tw,circ})}}{d\Omega_p}(\theta_p,\phi_p;\,\theta_c) = \mathcal{N}\frac{2\pi}{2J_i+1}\sum_{LL'pp'}i^{L-L'}(i\lambda)^{p-p'}[LL']\sum_{J_tJ_t'\kappa\kappa'}\mathcal{Z}\,[ll'][J_tJ_t']^{-1}\langle(\alpha_fJ_f,\epsilon\kappa)J_t||H_\gamma(pL)||\alpha_iJ_i\rangle\\ \times\,\langle(\alpha_fJ_f,\epsilon\kappa')J_t'||H_\gamma(p'L')||\alpha_iJ_i\rangle^*,\end{aligned} \tag{A6}$$

where

$$\begin{aligned}\mathcal{Z} = \sum_{\substack{M_iM_fm_sM\\ \mu\mu'M_tM_t'}}&\left(l0,\,\frac{1}{2}m_s\,\middle|\,jm_s\right)(J_fM_f,\,j\mu\,|\,J_tM_t)(J_iM_i,LM\,|\,J_tM_t)\left(l'0,\,\frac{1}{2}m_s\,\middle|\,j'm_s\right)(J_fM_f,\,j'\mu'\,|\,J_t'M_t')(J_iM_i,L'M\,|\,J_t'M_t')\\ &\times D^{j*}_{\mu m_s}(\hat{\boldsymbol{p}})D^{j'}_{\mu' m_s}(\hat{\boldsymbol{p}})d^L_{M\lambda}(\theta_c)\,d^{L'}_{M\lambda}(\theta_c).\end{aligned} \tag{A7}$$

The summation over the projections in (A7) can be performed analytically as follows. First we sum the product of four Clebsch-Gordan coefficients over $M_iM_fM_tM_t'$ using (A.91) of [37]:

$$\begin{aligned}&\sum_{M_iM_fM_tM_t'}(J_fM_f,\,j\mu\,|\,J_tM_t)\,(J_iM_i,LM\,|\,J_tM_t)(J_fM_f,\,j'\mu'\,|\,J_t'M_t')\,(J_iM_i,L'M\,|\,J_t'M_t')\\ &= (-1)^{J_t-J_t'+j-j'}\sum_{s\sigma}[sJ_tJ_t']^2\,[LL']^{-1}(j-\mu,s\sigma\,|\,L-M)(j'-\mu',s\sigma\,|\,L'-M)\begin{Bmatrix}J_f & J_t & j\\ L & s & J_i\end{Bmatrix}\begin{Bmatrix}J_f & J_t' & j'\\ L' & s & J_i\end{Bmatrix}.\end{aligned} \tag{A8}$$

Then, multiplying D-functions, we obtain

$$\begin{aligned}\mathcal{Z} = (-1)^{J_t-J_t'+j-j'}[sJ_tJ_t']^2\,[LL']^{-1}\sum_{sm_s}\sum_{JM_1M_2M}\sum_{\sigma\mu\mu'}(-1)^{m_s-\mu}(j-\mu,s\sigma\,|\,L-M)(j'-\mu',s\sigma\,|\,L'-M)\\ \times\,(j-\mu,j'\mu'\,|\,JM_1)(j-m_s,j'm_s\,|\,JM_2)\,D^J_{M_1M_2}(\hat{\boldsymbol{p}})\,\delta_{M_20}\left(l0,\,\frac{1}{2}m_s\,\middle|\,jm_s\right)\left(l'0,\,\frac{1}{2}m_s\,\middle|\,j'm_s\right)\\ \times\,\begin{Bmatrix}J_f & J_t & j\\ L & s & J_i\end{Bmatrix}\begin{Bmatrix}J_f & J_t' & j'\\ L' & s & J_i\end{Bmatrix}d^L_{M\lambda}(\theta_c)\,d^{L'}_{M\lambda}(\theta_c).\end{aligned} \tag{A9}$$

Next, we sum the products of three Clebsch-Gordan coefficients over $\mu\mu'\sigma$,

$$\sum_{\mu\mu'\sigma}(j-\mu, s\sigma\,|\,L-M)(j'-\mu', s\sigma\,|\,L'-M)(j-\mu, j'\mu'\,|\,JM_1)(-1)^{-\mu}$$
$$=(-1)^{s-j-j'-M}[LL'](L-M, L'M\,|\,J0)\begin{Bmatrix} L & L' & J \\ j' & j & s\end{Bmatrix}\delta_{M_1 0}, \tag{A10}$$

and over m_s,

$$\sum_{m_s}(-1)^{m_s}\left(l0, \frac{1}{2}m_s\middle|\, jm_s\right)\left(l'0, \frac{1}{2}m_s\middle|\, j'm_s\right)(j-m_s, j'm_s\,|\,J0)=(-1)^{j'+j+\frac{3}{2}}[jj'](l0, l'0\,|\,J0)\begin{Bmatrix} j & j' & J \\ l' & l & \frac{1}{2}\end{Bmatrix}. \tag{A11}$$

The result is

$$\mathcal{Z}=\sum_{sJM}(-1)^{J_t-J_t'+s-j'+j+\frac{3}{2}}(-1)^{J-M}[sJ_tJ_t']^2[jj'](l0, l'0\,|\,J0)(L-M, L'M\,|\,J0)$$
$$\times\begin{Bmatrix} J_f & j & J_t \\ L & J_i & s\end{Bmatrix}\begin{Bmatrix} J_f & j' & J_t' \\ L' & J_i & s\end{Bmatrix}\begin{Bmatrix} j & j' & J \\ L' & L & s\end{Bmatrix}\begin{Bmatrix} j & j' & J \\ l' & l & \frac{1}{2}\end{Bmatrix}d^L_{M\lambda}(\theta_c)\,d^{L'}_{M\lambda}(\theta_c)\,P_J(\cos\theta_p). \tag{A12}$$

After this, we sum over M,

$$\sum_M(-1)^{-M}(L-M, L'M\,|\,J0)\,d^L_{M\lambda}(\theta_c)\,d^{L'}_{M\lambda}(\theta_c)=\sum_M(-1)^{-\lambda}(L-M, L'M\,|\,J0)\,D^L_{-M-\lambda}(0,\theta_c,0)D^{L'}_{M\lambda}(0,\theta_c,0)$$
$$=(-1)^{-\lambda}(L-\lambda, L'\lambda\,|\,J0)\,P_J(\cos\theta_c), \tag{A13}$$

and over s,

$$\sum_s(-1)^s[s]^2\begin{Bmatrix} J_f & j & J_t \\ L & J_i & s\end{Bmatrix}\begin{Bmatrix} J_f & j' & J_t' \\ L' & J_i & s\end{Bmatrix}\begin{Bmatrix} j & j' & J \\ L' & L & s\end{Bmatrix}=(-1)^{-J_f-J_i-L-j-j'-L'-J_t-J-J_t'}\begin{Bmatrix} J_t & J & J_t' \\ j' & J_f & j\end{Bmatrix}\begin{Bmatrix} J_t & J & J_t' \\ L' & J_i & L\end{Bmatrix}. \tag{A14}$$

Collecting (A12)–(A14), we arrive at

$$\mathcal{Z}=(-1)^{J_i-J_f-\lambda-\frac{1}{2}}[J_tJ_t']^2\,[jj']\sum_J(l0, l'0\,|\,J0)\,(L\lambda, L'-\lambda\,|\,J0)\begin{Bmatrix} J_t & J_t' & J \\ j' & j & J_f\end{Bmatrix}\begin{Bmatrix} J_t & J_t' & J \\ L' & L & J_i\end{Bmatrix}\begin{Bmatrix} j & j' & J \\ l' & l & \frac{1}{2}\end{Bmatrix}$$
$$\times P_J(\cos\theta_p)\,P_J(\cos\theta_c). \tag{A15}$$

Substituting (A15) into (A6), we finally obtain the cross section as

$$\frac{d\sigma^{(\mathrm{tw,circ})}}{d\Omega_p}(\theta_p, \phi_p;\,\theta_c)=\mathcal{N}\frac{2\pi}{2J_i+1}\sum_J P_J(\cos\theta_p)P_J(\cos\theta_c)\sum_{\kappa\kappa' J_tJ_t'}\sum_{LL'pp'}i^{L-L'}[ll'J_tJ_t'LL'jj']$$
$$\times(i\lambda)^{p-p'}(-1)^{\lambda+J_i-J_f+\frac{1}{2}}\,(L\lambda, L'-\lambda\,|\,J0)\,(l0, l'0\,|\,J0)\begin{Bmatrix} j & j' & J \\ l' & l & \frac{1}{2}\end{Bmatrix}\begin{Bmatrix} J_t & J_t' & J \\ L' & L & J_i\end{Bmatrix}\begin{Bmatrix} J_t & J_t' & J \\ j' & j & J_f\end{Bmatrix}$$
$$\times\langle(\alpha_fJ_f, \epsilon\kappa)J_t||H_\gamma(pL)||\alpha_iJ_i\rangle\,\langle(\alpha_fJ_f, \epsilon\kappa')J_t'||H_\gamma(p'L')||\alpha_iJ_i\rangle^*. \tag{A16}$$

APPENDIX B: DIFFERENTIAL CROSS SECTION FOR LINEARLY POLARIZED BESSEL LIGHT

Recall that $\hat{\boldsymbol{p}}\equiv\{\phi_p, \theta_p, 0\}$ and $\hat{\boldsymbol{k}}\equiv\{\phi_k, \theta_c, 0\}$. To simplify Eq. (23), we first substitute the matrix elements (10). The result is

$$\frac{d\sigma^{(\mathrm{tw,lin})}}{d\Omega_p}(\theta_p, \phi_p;\,\theta_c)=\frac{\mathcal{N}}{2J_i+1}\sum_{M_iM_fm_s}\sum_{\lambda,\lambda'}\int d\phi_k\,e^{i(\lambda-\lambda')\phi_k}\sum_{\substack{LL'J_tJ_t'\\ pp'\kappa\kappa'}}\sum_{\substack{MM'\mu\mu'\\ M_tM_t'}}i^{L-L'}(i\lambda)^p(-i\lambda')^{p'}[ll'LL'][J_tJ_t']^{-1}\left(l0, \frac{1}{2}m_s\,|\,jm_s\right)$$
$$\times\left(l'0, \frac{1}{2}m_s\middle|\, j'm_s\right)(J_fM_f, j\mu\,|\,J_tM_t)\,(J_fM_f, j'\mu'\,|\,J_t'M_t')(J_iM_i, LM\,|\,J_tM_t)\,(J_iM_i, L'M'\,|\,J_t'M_t')$$
$$\times D^{j*}_{\mu m_s}(\hat{\boldsymbol{p}})\,D^{j'}_{\mu' m_s}(\hat{\boldsymbol{p}})\,D^L_{M\lambda}(\hat{\boldsymbol{k}})\,D^{L'*}_{M'\lambda'}(\hat{\boldsymbol{k}})\langle(\alpha_fJ_f, \epsilon\kappa)J_t||H_\gamma(pL)||\alpha_iJ_i\rangle\,\langle(\alpha_fJ_f, \epsilon\kappa')J_t'||H_\gamma(p'L')||\alpha_iJ_i\rangle^*. \tag{B1}$$

Now we perform the summations using the formulas

$$\sum_{M_i M_f M_t M_t'} (J_f M_f,\, j\mu \,|\, J_t M_t)\,(J_i M_i,\, LM \,|\, J_t M_t)(J_f M_f,\, j'\mu' \,|\, J_t' M_t')\,(J_i M_i,\, L'M' \,|\, J_t' M_t')$$

$$= (-1)^{J_f - J_i - L + L' + j + j' - M' - \mu'} [J_t J_t']^2 \sum_{s\sigma} (L' - M',\, LM \,|\, s\sigma)(j' - \mu',\, j\mu \,|\, s\sigma) \begin{Bmatrix} J_t & J_t' & s \\ L' & L & J_i \end{Bmatrix} \begin{Bmatrix} J_t & J_t' & s \\ j' & j & J_f \end{Bmatrix}, \tag{B2}$$

$$\sum_{\mu\mu'} (-1)^{-\mu'} (j' - \mu',\, j\mu \,|\, s\sigma) D^{j*}_{\mu m_s}(\hat{\boldsymbol{p}})\, D^{j'}_{\mu' m_s}(\hat{\boldsymbol{p}}) = (-1)^{m_s + 2\sigma} (j - m_s,\, j' m_s \,|\, s0) D^{s}_{0\sigma}(\hat{\boldsymbol{p}}^{-1}), \tag{B3}$$

$$\sum_{MM'} (-1)^{-M'} (L' - M',\, LM \,|\, s\sigma) D^{L}_{M\lambda}(\hat{\boldsymbol{k}})\, D^{L'*}_{M'\lambda'}(\hat{\boldsymbol{k}}) = (-1)^{\lambda - \sigma} (L' - \lambda',\, L\lambda \,|\, s\lambda - \lambda') D^{s}_{\lambda - \lambda' \sigma}(\hat{\boldsymbol{k}}^{-1}). \tag{B4}$$

Here we introduced the notations $\hat{\boldsymbol{p}}^{-1} \equiv \{0, \theta_p, \phi_p\}$ and $\hat{\boldsymbol{k}}^{-1} \equiv \{0, \theta_c, \phi_k\}$,

$$\sum_{m_s} (-1)^{m_s} \left(l0,\, \frac{1}{2} m_s \,\middle|\, j m_s \right) \left(l'0,\, \frac{1}{2} m_s \,\middle|\, j' m_s \right) (j - m_s,\, j' m_s \,|\, s0) = (-1)^{j' + j + \frac{3}{2}} [j j'] \times (l0,\, l'0 \,|\, s0) \begin{Bmatrix} j & j' & s \\ l' & l & \frac{1}{2} \end{Bmatrix}. \tag{B5}$$

Finally, we use the integral

$$\int d\phi_k\, e^{i(\lambda - \lambda')\phi_k} D^{s}_{\lambda - \lambda' \sigma}(\hat{\boldsymbol{k}}^{-1}) = 2\pi\, d^{s}_{\sigma\sigma}(\theta_c) \delta_{\sigma, \lambda - \lambda'} \tag{B6}$$

and note that

$$D^{s}_{0\sigma}(\hat{\boldsymbol{p}}^{-1}) = (-1)^{\sigma} \sqrt{\frac{4\pi}{2s + 1}} Y^{*}_{s\sigma}(\hat{\boldsymbol{p}}). \tag{B7}$$

Collecting (B1)–(B7) and replacing the summation indices $s\sigma \to JM$, we obtain

$$\frac{d\sigma^{(\mathrm{tw,lin})}}{d\Omega_p}(\theta_p, \phi_p;\, \theta_c)$$

$$= \mathcal{N} \frac{2\pi}{2J_i + 1} \sum_{J} \sum_{M = 0, \pm 2} \sqrt{\frac{4\pi}{2J + 1}} Y^{*}_{JM}(\theta_p, \phi_p)\, d^{J}_{MM}(\theta_c) \sum_{\lambda, \lambda'} \delta_{M, \lambda - \lambda'}$$

$$\times \sum_{\kappa\kappa' J_t J_t'} \sum_{LL' pp'} i^{L - L'} (i\lambda)^{p} (-i\lambda')^{p'} (-1)^{\lambda + J_i - J_f + \frac{1}{2}} [l l' L L' J_t J_t' j j'] (l0,\, l'0 \,|\, J0)(L\lambda,\, L' - \lambda' \,|\, JM)$$

$$\times \begin{Bmatrix} j & j' & J \\ l' & l & \frac{1}{2} \end{Bmatrix} \begin{Bmatrix} J_t & J_t' & J \\ L' & L & J_i \end{Bmatrix} \begin{Bmatrix} J_t & J_t' & J \\ j' & j & J_f \end{Bmatrix} \langle (\alpha_f J_f, \epsilon\kappa) J_t || H_\gamma(pL) || \alpha_i J_i \rangle \, \langle (\alpha_f J_f, \epsilon\kappa') J_t' || H_\gamma(p' L') || \alpha_i J_i \rangle^{*}. \tag{B8}$$

[1] J. Bahrdt, K. Holldack, P. Kuske, R. Müller, M. Scheer, and P. Schmid, First Observation of Photons Carrying Orbital Angular Momentum in Undulator Radiation, Phys. Rev. Lett. **111**, 034801 (2013).

[2] G. Molina-Terriza, J. P. Torres, and L. Torner, Twisted photons, Nat. Phys. **3**, 305 (2007).

[3] A. Bekshaev, K. Y. Bliokh, and M. Soskin, Internal flows and energy circulation in light beams, J. Opt. **13**, 053001 (2011).

[4] K. Sueda, G. Miyaji, N. Miyanaga, and M. Nakatsuka, Laguerre-Gaussian beam generated with a multilevel spiral phase plate for high intensity laser pulses, Opt. Express **12**, 3548 (2004).

[5] M. Beijersbergen, R. Coerwinkel, M. Kristensen, and J. Woerdman, Helical-wavefront laser beams produced with a spiral phaseplate, Opt. Commun. **112**, 321 (1994).

[6] N. R. Heckenberg, R. McDuff, C. P. Smith, and A. G. White, Generation of optical phase singularities by computer-generated holograms, Opt. Lett. **17**, 221 (1992).

[7] E. Karimi, B. Piccirillo, E. Nagali, L. Marrucci, and E. Santamato, Efficient generation and sorting of orbital angular momentum eigenmodes of light by thermally tuned q-plates, Appl. Phys. Lett. **94**, 231124 (2009).

[8] J. Arlt and K. Dholakia, Generation of high-order Bessel beams by use of an axicon, Opt. Commun. **177**, 297 (2000).

[9] X. Cai, J. Wang, M. J. Strain, B. Johnson-Morris, J. Zhu, M. Sorel, J. L. O'Brien, M. G. Thompson, and S. Yu, Integrated compact optical vortex beam emitters, Science **338**, 363 (2012).

[10] H. Yang, Z. Xie, H. He, Q. Zhang, and X. Yuan, A perspective on twisted light from on-chip devices, APL Photon. **6**, 110901 (2021).

[11] A. G. Peele, P. J. McMahon, D. Paterson, C. Q. Tran, A. P. Mancuso, K. A. Nugent, J. P. Hayes, E. Harvey, B. Lai, and I. McNulty, Observation of an x-ray vortex, Opt. Lett. **27**, 1752 (2002).

[12] S. Sasaki and I. McNulty, Proposal for Generating Brilliant X-Ray Beams Carrying Orbital Angular Momentum, Phys. Rev. Lett. **100**, 124801 (2008).

[13] E. Hemsing, A. Marinelli, and J. B. Rosenzweig, Generating Optical Orbital Angular Momentum in a High-Gain Free-Electron Laser at the First Harmonic, Phys. Rev. Lett. **106**, 164803 (2011).

[14] U. D. Jentschura and V. G. Serbo, Compton upconversion of twisted photons: Backscattering of particles with nonplanar wave functions, Eur. Phys. J. C **71**, 1571 (2011).

[15] U. D. Jentschura and V. G. Serbo, Generation of High-Energy Photons with Large Orbital Angular Momentum by Compton Backscattering, Phys. Rev. Lett. **106**, 013001 (2011).

[16] J. He, X. Wang, D. Hu, J. Ye, S. Feng, Q. Kan, and Y. Zhang, Generation and evolution of the terahertz vortex beam, Opt. Express **21**, 20230 (2013).

[17] Y. Shen, G. T. Campbell, B. Hage, H. Zou, B. C. Buchler, and P. K. Lam, Generation and interferometric analysis of high charge optical vortices, J. Opt. **15**, 044005 (2013).

[18] P. R. Ribič, D. Gauthier, and G. De Ninno, Generation of Coherent Extreme-Ultraviolet Radiation Carrying Orbital Angular Momentum, Phys. Rev. Lett. **112**, 203602 (2014).

[19] C. Hernández-García, L. Rego, J. San Román, A. Picón, and L. Plaja, Attosecond twisted beams from high-order harmonic generation driven by optical vortices, High Power Laser Sci. Eng. **5**, e3 (2017).

[20] L. Allen, M. W. Beijersbergen, R. J. C. Spreeuw, and J. P. Woerdman, Orbital angular momentum of light and the transformation of Laguerre-Gaussian laser modes, Phys. Rev. A **45**, 8185 (1992).

[21] L. Allen, M. Padgett, and M. Babiker, *IV The Orbital Angular Momentum of Light* (Elsevier, New York, 1999), pp. 291–372.

[22] J. Durnin, Exact solutions for nondiffracting beams. I. The scalar theory, J. Opt. Soc. Am. A **4**, 651 (1987).

[23] J. Durnin, J. J. Miceli, and J. H. Eberly, Diffraction-free beams, Phys. Rev. Lett. **58**, 1499 (1987).

[24] M. Babiker, D. L. Andrews, and V. E. Lembessis, Atoms in complex twisted light, J. Opt. **21**, 013001 (2019).

[25] A. Surzhykov, D. Seipt, and S. Fritzsche, Probing the energy flow in bessel light beams using atomic photoionization, Phys. Rev. A **94**, 033420 (2016).

[26] V. P. Kosheleva, V. A. Zaytsev, R. A. Müller, A. Surzhykov, and S. Fritzsche, Resonant two-photon ionization of atoms by twisted and plane-wave light, Phys. Rev. A **102**, 063115 (2020).

[27] S. Ramakrishna, J. Hofbrucker, and S. Fritzsche, Photoexcitation of atoms by cylindrically polarized Laguerre-Gaussian beams, Phys. Rev. A **105**, 033103 (2022).

[28] F. Araoka, T. Verbiest, K. Clays, and A. Persoons, Interactions of twisted light with chiral molecules: An experimental investigation, Phys. Rev. A **71**, 055401 (2005).

[29] A. A. Peshkov, S. Fritzsche, and A. Surzhykov, Ionization of h_2^+ molecular ions by twisted bessel light, Phys. Rev. A **92**, 043415 (2015).

[30] O. Matula, A. G. Hayrapetyan, V. G. Serbo, A. Surzhykov, and S. Fritzsche, Atomic ionization of hydrogen-like ions by twisted photons: Angular distribution of emitted electrons, J. Phys. B: At. Mol. Opt. Phys. **46**, 205002 (2013).

[31] D. Seipt, R. A. Müller, A. Surzhykov, and S. Fritzsche, Two-color above-threshold ionization of atoms and ions in XUV Bessel beams and intense laser light, Phys. Rev. A **94**, 053420 (2016).

[32] A. Picón, J. Mompart, J. R. V. de Aldana, L. Plaja, G. F. Calvo, and L. Roso, Photoionization with orbital angular momentum beams, Opt. Express **18**, 3660 (2010).

[33] J. W. Cooper, Multipole corrections to the angular distribution of photoelectrons at low energies, Phys. Rev. A **42**, 6942 (1990).

[34] J. W. Cooper, Photoelectron-angular-distribution parameters for rare-gas subshells, Phys. Rev. A **47**, 1841 (1993).

[35] S. A.-L. Schulz, S. Fritzsche, R. A. Müller, and A. Surzhykov, Modification of multipole transitions by twisted light, Phys. Rev. A **100**, 043416 (2019).

[36] M. E. Rose, *Elementary Theory of Angular Momentum* (Wiley, New York, 1957).

[37] V. V. Balashov, A. N. Grum-Grzhimailo, and N. M. Kabachnik, *Polarization and Correlation Phenomena in Atomic Collisions* (Springer, Boston, MA, 2000).

[38] J. Eichler and W. E. Meyerhof, Chapter 4 - Relativistic electron motion, in *Relativistic Atomic Collisions*, edited by J. Eichler and W. E. Meyerhof (Academic Press, San Diego, 1995), pp. 61–96.

[39] W. Greiner, *Relativistic Quantum Mechanics. Wave Equations* (Springer, Berlin, 1990).

[40] H. M. Scholz-Marggraf, S. Fritzsche, V. G. Serbo, A. Afanasev, and A. Surzhykov, Absorption of twisted light by hydrogenlike atoms, Phys. Rev. A **90**, 013425 (2014).

[41] S. A.-L. Schulz, A. A. Peshkov, R. A. Müller, R. Lange, N. Huntemann, C. Tamm, E. Peik, and A. Surzhykov, Generalized excitation of atomic multipole transitions by twisted light modes, Phys. Rev. A **102**, 012812 (2020).

[42] G. F. Quinteiro, D. E. Reiter, and T. Kuhn, Formulation of the twisted-light–matter interaction at the phase singularity: The twisted-light gauge, Phys. Rev. A **91**, 033808 (2015).

[43] O. Zatsarinny, BSR: *B*-spline atomic *R*-matrix codes, Comput. Phys. Commun. **174**, 273 (2006).

[44] C. F. Fischer, T. Brage, and P. Johnsson, *Computational Atomic Structure: An MCHF Approach* (IOP, Bristol, 1997).

[45] B. Krässig, E. P. Kanter, S. H. Southworth, R. Guillemin, O. Hemmers, D. W. Lindle, R. Wehlitz, and N. L. S. Martin, Photoexcitation of a Dipole-Forbidden Resonance in Helium, Phys. Rev. Lett. **88**, 203002 (2002).

[46] L. Argenti and R. Moccia, Nondipole effects in helium photoionization, J. Phys. B: At. Mol. Opt. Phys. **43**, 235006 (2010).

[47] P. S. Shaw, U. Arp, and S. H. Southworth, Measuring nondipolar asymmetries of photoelectron angular distributions, Phys. Rev. A **54**, 1463 (1996).

[48] https://rscf.ru/en/project/21-42-04412/.